951 (1954).
[13]J. C. Slater, Phys. Rev. 81, 385 (1951).
[14]R. M. Sternheimer, Phys. Rev. 84, 244 (1951); 146, 140 (1966); H. M. Foley, R. M. Sternheimer, and D. Tycko, *ibid.* 93, 734 (1954).
[15]I. I. Glembotskii, V. V. Kibartas, and A. P. Iutsis, Zh. Eksperim. i Teor. Fiz. 29, 617 (1955) [Sov. Phys. JETP 2, 476 (1956)].
[16]H. Lew and G. Wessel, Phys. Rev. 90, 1 (1953).
[17]H. F. Schaefer, III, R. A. Klemm, and F. E. Harris, Phys. Rev. 176, 49 (1968).
[18]R. K. Nesbet, Phys. Rev. A 2, 1208 (1970).
[19]S. Larsson, Phys. Rev. A 2, 1248 (1970).
[20]G. A. Sawatzky and J. Hupkes, Phys. Rev. Letters 25, 100 (1970).
[21]R. R. Sharma, Phys. Rev. Letters 25, 1622 (1970).
[22]T. P. Das and R. Bersohn, Phys. Rev. 102, 733 (1956).
[23]R. M. Sternheimer, Phys. Rev. 115, 1198 (1959).

PHYSICAL REVIEW A VOLUME 4, NUMBER 5 NOVEMBER 1971

L X-Ray Transition Probabilities in Elements with $Z \geq 57$

S. I. Salem, R. T. Tsutsui, and B. A. Rabbani
Department of Physics and Astronomy, California State College, Long Beach, California 90801
(Received 23 April 1971)

The $L\beta_3/L\beta_4$, $L\gamma_1/L\beta_1$, $L\alpha_2/L\alpha_1$, $L\beta_{2,15}/L\alpha_1$ and the $L\beta_{2,15}/L\alpha_2$ transition probabilities have been measured for some 27 elements ranging in atomic number from $_{57}$La to $_{92}$U. Other *L* transitions have also been measured for a smaller number of elements in the same range of atomic numbers. This has been accomplished by bombarding these elements with a constant energy electron beam and measuring their x-ray emission spectrum. The measured ratios are compared with the most recent calculation based on a relativistic Hartree-Fock-Slater (RHFS) potential, and screened Coulomb potential. In general, the form of the dependence of these ratios on atomic number predicted by calculations based on a RHFS potential is favored and the agreement between theory and experiment ranges from excellent for the $L\alpha_2/L\alpha_1$ ratio to a discrepancy of about 22% in the $L\beta_{2,15}/L\alpha_1$ ratio for elements of large atomic number.

INTRODUCTION

Recent interest in measuring relative x-ray transition probabilities has been confined to the relatively simple *K* series. The *L* x-ray transition probabilities of elements with atomic number $57 \leq Z \leq 72$ have never been measured before, and work in this region proved to be very informative in terms of testing the different theoretical models used in calculating the relative probability of these transitions.

Early measurements of transition probability of the *L* x-ray group comprise the work of Jönsson,[1] Allison,[2] Hicks,[3] and Andrew.[4] Their results have been tabulated by Compton and Allison.[5] More recent measurements include the work of Wyckoff and Davidson,[6] Victor,[7] Goldberg,[8] and Rao *et al.*[9] None of the measurements cover a large enough number of elements to establish reasonable correlation with theoretical calculations, and in many instances the discrepancies between these results are of large magnitude.

Relativistic calculations of x-ray transition probabilities were carried out by Massey and Burhop,[10] Laskar,[11] Payne and Levinger,[12] Asaad,[13] Taylor and Payne,[14] and more recently by Babushkin,[15] Scofield,[16] and Rosner and Bhalla.[17] All these calculations except those of Asaad, Scofield, and Rosner and Bhalla are based on a Coulomb potential. Babushkin carried out his calculations using a Coulomb potential with and without allowance for screening; he took into account the electron screening effect as prescribed by Slater[18] and by Burns.[19] Of Babushkin's calculations, those based on a potential screened by Burns's prescription show better agreement with experimental values,[20,21] and these are later compared with the results of this paper. Babushkin's numerical values are given as intensity ratios rather than relative transition probabilities and were transformed to transition probabilities by the relation

$$P_i = I_i/\hbar\omega_i \,, \tag{1}$$

where the subscript i indicates a given transition of energy $\hbar\omega_i$.

Scofield, and Rosner and Bhalla assumed that the orbital electrons are in a relativistic Hartree-Fock-Slater potential[22] (RHFS):

$$V(r) = -Ze^2/r + (e^2/r)\int_0^r 4\pi r'^2\rho(r')\,dr' + e^2\int_r^\infty 4\pi r'\rho(r')\,dr' - e^2[(81/8\pi)\rho(r)]^{1/3} \,. \tag{2}$$

The effect of the finite size of the nucleus was neglected by Scofield, and was calculated and ne-

glected by Babushkin on the basis that it amounts only to a fraction of one percent. Rosner and Bhalla included such an effect without explicitly referring to its magnitude. They all included the effect of retardation in their calculations. The numerical results of Rosner and Bhalla agree with those of Scofield to within three significant figures.

The extensive experimental work on $K\beta/K\alpha$ transition probabilities[20,23,24] did not resolve the discrepancy between the results of calculations based on a Coulomb potential and those based on a RHFS potential in the region $20 \leq Z \leq 30$. Similar discrepancies, but of a larger magnitude, occur in the $L\beta_{2,15}/L\alpha_1$ and in the $L\gamma_1/L\beta_1$ transition probability ratios in the region $58 \leq Z \leq 71$. The magnitude of such discrepancies in the L spectra is roughly an order of magnitude greater than experimental uncertainties, and the determination of these ratios in this region should provide a reasonable concept of the form of the potential in which these transitions take place.

EXPERIMENTAL

The elements studied varied in purity from 99.99% for gold and tungsten to 99.5% for osmium. The 99.9%-pure rare-earth elements were foils 0.13 mm thick. The electron beam used in exciting the target elements was provided by a 74-W filament fitted in a stainless steel focussing cup. The filament is heated by an insulating transformer. The electron energy is provided by a power supply connected in series with a voltage line regulator and a ripple suppressor, and delivers a steady voltage with less than 0.3% ripple at a full load of 120 keV and 30 mA. The energy of the electron beam was maintained at 25 keV during the bombardment of all the elements with $Z \leq 83$, and at 40 keV during the study of $_{90}$Th and $_{92}$U. The current was maintained at 1.0 mA.

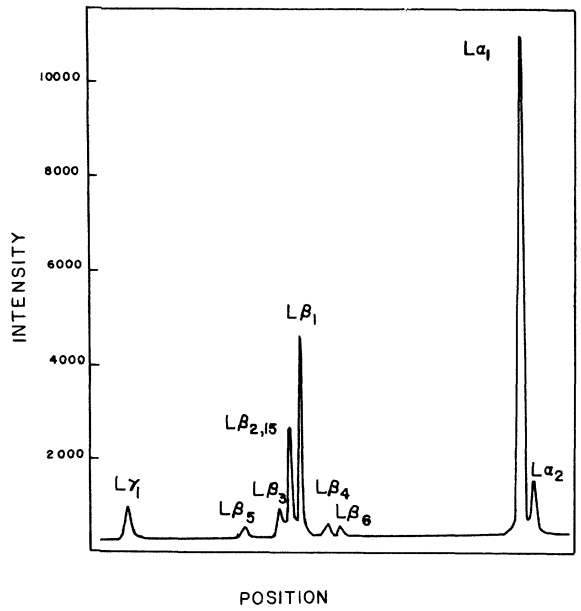

FIG. 1. Observed L x-ray lines of mercury, designated by the Siegbahn notations.

TABLE I. $L\beta_3/L\beta_4$ $[(L_I - M_{III})/(L_I - M_{II})]$ transition probability ratio. The third column is the ratio of the MPV to Scofield's theoretical values.

Elements	Measured values	MPV	MPV / Theory
$_{57}$La	1.53	1.54	1.00
$_{58}$Ce	1.57	1.54	1.01
$_{59}$Pr		1.54	1.02
$_{60}$Nd		1.55	1.05
$_{62}$Sm		1.55	1.06
$_{64}$Gd	1.60	1.54	1.07
$_{65}$Tb	1.49	1.54	1.09
$_{66}$Dy	1.60	1.54	1.10
$_{67}$Ho	1.54	1.53	1.11
$_{68}$Er	1.42	1.52	1.12
$_{69}$Tm	1.51	1.51	1.12
$_{70}$Yb	1.53	1.50	1.14
$_{71}$Lu	1.43	1.49	1.14
$_{72}$Hf	1.44	1.48	1.14
$_{73}$Ta	1.47	1.47	1.15
$_{74}$W	1.37	1.45	1.16
$_{75}$Re	1.49	1.44	1.16
$_{76}$Os	1.36	1.42	1.16
$_{77}$Ir	1.43	1.40	1.17
$_{78}$Pt		1.38	1.18
$_{79}$Au		1.36	1.18
$_{80}$Hg	1.42	1.34	1.19
$_{81}$Tl	1.35	1.31	1.18
$_{82}$Pb	1.38	1.29	1.18
$_{83}$Bi	1.24	1.26	1.17
$_{90}$Th	1.00	1.05	1.15
$_{92}$U	0.96	0.975	1.13

A modified high-angle goniometer was used to scan over the region of interest, and for each sample the line intensity was also measured in steps of 0.005° in the Bragg angle 2θ. At least four runs for each element were recorded and averaged. A typical spectrum is shown in Fig. 1.

Most of the elements used in this work were in the form of metal foils varying in thickness from 0.5 to 0.13 mm. Backing was provided for all the foils before being fitted to the water-cooled anode assembly. Triple-distilled mercury was put in a brass container and osmium powder was press-packed in a similar container. Elements of low melting points, $_{81}$Tl, $_{82}$Pb and $_{83}$Bi, were melted in a brass container and their surfaces were smoothed and cleaned; they were then introduced into the vacuum chamber.

The foils of the rare-earth elements and those of $_{90}$Th and $_{92}$U were placed at the surface of a dish filled with $_{31}$Ga. The water-cooled melt gallium

proved to be very satisfactory in keeping the thin foils from evaporating under electron bombardment. At the early stages of this work, the foils were floated on $_{80}$Hg, but mercury was replaced with gallium when it was found that most rare-earth elements react with mercury when heated.

Although the ratio of the physical areas under the curves obtained by stepping over the diffraction peaks is of more physical significance, the ratio of the peak intensities was considered more reliable in determining the transition probabilities as it is less susceptible to instrumental factors. It should be pointed out that the natural widths of the compared characteristic lines are very nearly the same for the same elements, and accordingly, the ratio of the peak intensities should be very nearly the same as the ratio of the physical areas under the curves. Furthermore, the reported physical widths of the L x-ray series involve large uncertainties

Irregularities in the shape of the $L\beta_{2,15}$ and $L\gamma_1$ lines of the rare-earth elements, $58 \leq Z \leq 71$, were observed and were accounted for by comparing areas of irregularities to the areas of the symmetric portion of the characteristic lines. These irregularities seem to be quite different from reported asymmetries observed in the $K\alpha_1$ and $K\alpha_2$ x-ray lines of the elements[25] $35 \geq Z \geq 19$. [A study of the shapes of these lines has been published elsewhere (Ref. 25a)].

In elements where two characteristic lines were not far enough apart for the peak of one to be completely free of contribution from the Lorentzian tail of the other, the two lines were unfolded and contribution from their over-extended tails measured and their effect eliminated. Characteristic lines which were not well resolved, $L\beta_1$ and $L\beta_2$ in $_{82}$Pb, for example, are not reported.

At high atomic number where the $L\beta_{15}$ and $L\beta_2$ were resolved, the intensity of the $L\beta_{15}$ which amounts to some 3 to 4% of the $L\beta_2$ intensity was simply added to the $L\beta_2$.

Whenever a relatively weak line is too close to a strong line as the $L\beta_4$ is to the $L\beta_1$ in $_{60}$Nd, the magnitude of the $L\beta_4$ line was determined from the most probable value of $L\beta_3/L\beta_4$ transition probability ratio (Table I) and the contribution of the $L\beta_4$ subtracted from $L\beta_1$. In such cases, transition probability ratios involving the weak lines were not reported.

To reduce the effect of self-absorption, which is complicated by photo-ionization,[26] the energy of the exciting electrons was kept as close to the L_1 ionization energy of the sample as was practically possible. The mean depth of formation of L characteristic lines was calculated from previously measured values[27] and the fact that such depth is inversely proportional to the electron density in the bombarded sample. Corrections were made for the

TABLE II. $L\gamma_1/L\beta_1$ $[(L_{II}-N_{IV})/(L_{II}-M_{IV})]$ transition probability ratio. The third column is the ratio of the MPV to Scofield's theoretical values.

Elements	Measured values	MPV	MPV / Theory
$_{57}$La	0.176	0.169	1.04
$_{58}$Ce	0.158	0.170	1.03
$_{59}$Pr		0.170	1.02
$_{60}$Nd	0.173	0.169	1.01
$_{62}$Sm	0.170	0.166	0.965
$_{64}$Gd	0.162	0.163	0.942
$_{65}$Tb	0.163	0.162	0.931
$_{66}$Dy	0.158	0.162	0.931
$_{67}$Ho	0.171	0.162	0.931
$_{68}$Er	0.163	0.163	0.931
$_{69}$Tm	0.146	0.165	0.938
$_{70}$Yb	0.164	0.168	0.944
$_{71}$Lu	0.200	0.172	0.961
$_{72}$Hf	0.166	0.176	0.978
$_{73}$Ta	0.170	0.181	0.984
$_{74}$W	0.174	0.186	1.00
$_{75}$Re	0.220	0.192	1.02
$_{76}$Os	0.196	0.198	1.03
$_{77}$Ir	0.197	0.203	1.04
$_{78}$Pt	0.226	0.207	1.06
$_{79}$Au	0.188	0.211	1.07
$_{80}$Hg	0.227	0.215	1.08
$_{81}$Tl	0.195	0.217	1.07
$_{82}$Pb		0.218	1.07
$_{83}$Bi	0.232	0.218	1.05
$_{90}$Th	0.233	0.235	1.06
$_{92}$U	0.253	0.237	1.05

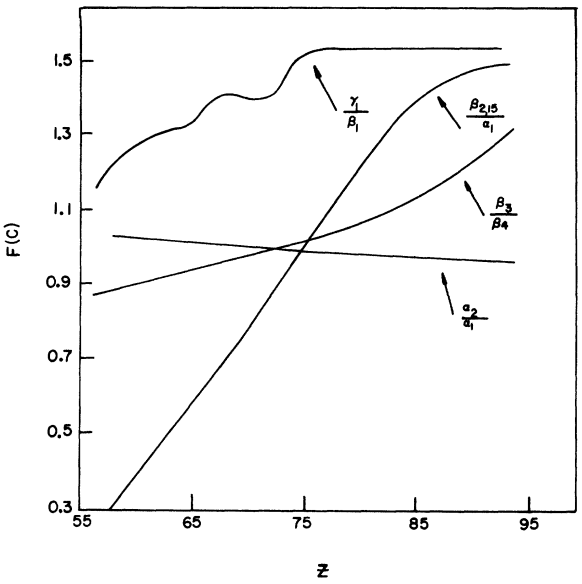

FIG. 2. Calculated correction factors applied to the indicated transition probability ratios. These include differential absorption, reflectivity of the crystal, and the efficiency of the detector.

TABLE III. $L\alpha_2/L\alpha_1$ and $L\beta_{2,15}/L\alpha_1$ transition probability ratios (for legend, see Table I).

Elements	$\frac{L\alpha_2}{L\alpha_1}, \left(\frac{L_{III}-M_{IV}}{L_{III}-M_V}\right)$ Measured values	MPV	MPV / Theory	$\frac{L\beta_{2,15}}{L\alpha_1}, \left(\frac{L_{III}-N_{IV,V}}{L_{III}-M_V}\right)$ Measured values	MPV	MPV / Theory
$_{57}$La	0.114	0.107	0.947	0.212	0.212	1.19
$_{58}$Ce	0.108	0.108	0.956		0.208	1.16
$_{59}$Pr	0.110	0.108	0.956	0.204	0.210	1.15
$_{60}$Nd	0.104	0.109	0.965	0.225	0.215	1.17
$_{62}$Sm	0.105	0.110	0.973	0.214	0.222	1.19
$_{64}$Gd	0.101	0.111	0.980	0.224	0.216	1.15
$_{65}$Tb	0.115	0.111	0.981	0.198	0.207	1.10
$_{66}$Dy	0.103	0.111	0.981	0.196	0.195	1.04
$_{67}$Ho	0.116	0.111	0.981	0.174	0.182	0.968
$_{68}$Er	0.115	0.112	0.990	0.196	0.171	0.910
$_{69}$Tm	0.113	0.112	0.990	0.150	0.163	0.867
$_{70}$Yb	0.113	0.112	0.995	0.156	0.163	0.862
$_{71}$Lu	0.117	0.112	0.991	0.179	0.175	0.921
$_{72}$Hf	0.116	0.112	0.987	0.192	0.180	0.942
$_{73}$Ta	0.113	0.112	0.983	0.188	0.193	1.00
$_{74}$W	0.113	0.112	0.986	0.180	0.208	1.06
$_{75}$Re	0.110	0.112	0.987	0.219	0.223	1.12
$_{76}$Os	0.111	0.112	0.987	0.269	0.236	1.18
$_{77}$Ir	0.111	0.112	0.987	0.250	0.247	1.21
$_{78}$Pt	0.112	0.112	0.987	0.246	0.255	1.24
$_{79}$Au	0.116	0.112	0.985	0.251	0.256	1.23
$_{80}$Hg	0.107	0.112	0.986	0.266	0.257	1.22
$_{81}$Tl	0.112	0.111	0.981	0.269	0.258	1.22
$_{82}$Pb	0.114	0.111	0.979		0.259	1.21
$_{83}$Bi	0.107	0.111	0.979	0.227	0.260	1.20
$_{90}$Th	0.110	0.108	0.948	0.246	0.285	1.24
$_{92}$U	0.105	0.107	0.941	0.315	0.290	1.24

counter recovery time, for differential self-absorption, absorption in the $_4$Be x-ray tube window and the air path, and for the reflectivity R_c of the calcite crystal and the efficiency E_c of the G-M $_{54}$Xe-filled counter as a function of the photon energy. The correction factor is

$$F(c) = (R_c E_c)^{-1} \, e^{+\Sigma_j \mu_j \rho_j t_j} \, e^{\mu_t \rho_t t_t \csc\psi} , \qquad (3)$$

where μ_j, ρ_j, and t_j are, respectively, the mass absorption coefficients, the mass density, and the thickness of the materials traversed by the photons before reaching the counter. μ_t is the mass absorption coefficient of the target material for its own characteristic lines, ρ_t is the target mass density, t_t is the mean depth of formation of characteristic x-ray lines, and ψ is the take-off angle. The values of the mass absorption coefficient used were those tabulated by McMaster *et al.*,[28] and the values of R_c were taken from Ref. 5. Equation (3) was computer-solved for the reported transition prob-

TABLE IV. Measured transition probability ratios and their theoretical values from Ref. 16.

Elements	$\frac{L\beta_5}{L\alpha_1}, \left(\frac{L_{III}-O_{IV,V}}{L_{III}-M_V}\right)$ Expt.	Theor.	$\frac{L\beta_6}{L\alpha_1}, \left(\frac{L_{III}-N_I}{L_{III}-M_V}\right)$ Expt.	Theor.	$\frac{L\gamma_2}{L\beta_4}, \left(\frac{L_I-N_{II}}{L_I-M_{IV}}\right)$ Expt.	Theor.
$_{75}$Re			0.012±0.002	0.0128		
$_{77}$Ir	0.015±0.004	0.0125				
$_{78}$Pt	0.017±0.004	0.0156			0.31±0.06	0.253
$_{79}$Au	0.022±0.0045	0.0185	0.012±0.003	0.0137		
$_{80}$Hg			0.016±0.003	0.0140		
$_{81}$Tl			0.014±0.003	0.0143	0.29±0.06	0.256
$_{82}$Pb	0.035±0.006	0.0257	0.014±0.003	0.0145	0.37±0.07	0.257
$_{83}$Bi			0.020±0.004	0.0147	0.40±0.08	0.258
$_{92}$U	0.059±0.01	0.044				

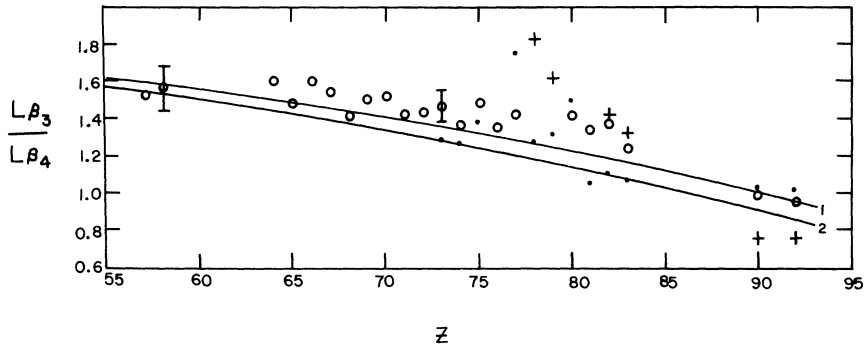

FIG. 3. $L\beta_3/L\beta_4$ transition probability ratio as a function of the atomic number Z. Curve 1 is from Babushkin's calculation based on a Coulomb potential screened by Burns's prescription. Curve 2 is from Scofield's calculations based on a RHFS potential. The plus signs are from Victor, Ref. 7; the solid dots are from Goldberg, Ref. 8; and the open circles are from the present work. The bars indicate percent error.

ability ratios of all the elements studied. Smooth curves through the calculated points are shown in Fig. 2. Corrections for the ratios given in Table IV were also made but their correction factors are not shown.

Several different sources of errors were considered. These include (i) counting statistics, (ii) systematic errors, (iii) voltage instabilities, (iv) tungsten contamination of the anode from heated filament, (v) spectrum unfolding, and (vi) errors in calculating $F(c)$. To reduce statistical errors, the spectrum of each element was measured several times and the average values are reported. Systematic errors were also reduced by stepping the detector for a complete run in the increasing direction of the Bragg angle and for the following run in the opposite direction. An error analysis was carried out for all measured ratios. These were found out to be about 5% in the $L\alpha_2/L\alpha_1$ and $L\beta_3/L\beta_4$ ratios for most elements except when unfolding of these characteristic lines became necessary. In such cases, the error was estimated at about 6%.

Combined errors of about 12% were calculated for the ratios $L\beta_{2,15}/L\alpha_1$, $L\beta_{2,15}/L\alpha_2$, and $L\gamma_1/L\beta_1$. The magnitudes of these errors are indicated by error bars in the appropriate graphs. Similarly calculated errors are reported in Table IV.

RESULTS AND DISCUSSION

Previously published experimental results on L x-ray radiative transitions, except those of Victor[7] and Goldberg,[8] were normalized relative to $L\alpha_1$. Because of the difference in the ionization potential of the three L subshells and the dependence of the ionization cross section on the net energy of the ionizing particle, such results are energy dependent, and relative transition probabilities involving different L subshells are very sensitive to the energy of the ionizing particle at low energies. Furthermore, even at high energies, $E_{\text{inc}} - I \simeq E_{\text{inc}}$, such ratios would not give true atomic transition probabilities because of the Auger and Coster-Kronig transitions.[29]

The results of this work are presented in four different tables: Tables I, II, and III contain transitions to L_{I}, L_{II}, and L_{III} subshells, respectively. Each table contains the corrected measured values, the most probable values (MPV), and the ratio of MPV to Scofield's theoretical values. The MPV were obtained from a least-squares computer fitted to the experimental points. Table IV contains other corrected measured values of transition prob-

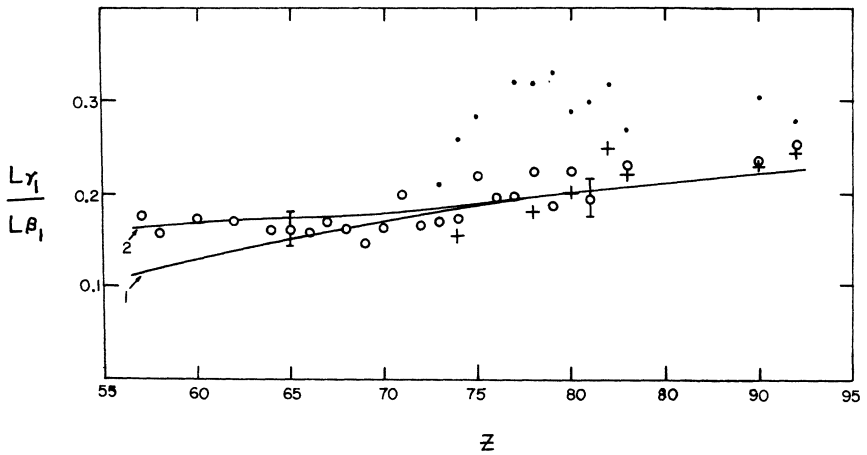

FIG. 4. $L\gamma_1/L\beta_1$ transition probability ratio as a function of atomic number Z. The curve labels and the symbols have the same designation as in Fig. 3.

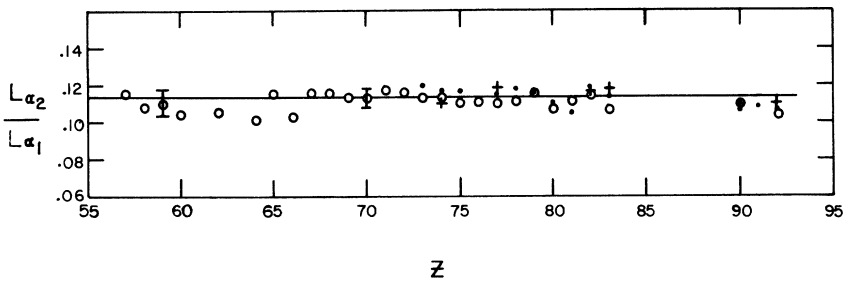

FIG. 5. Straight line is from Scofield's calculation, Ref. 16. For the rest of the legend, see Fig. 3.

abilities and Scofield's corresponding theoretical values. The transition probability ratios listed in Table IV, for one reason or the other, were not measured for a large enough number of elements to justify their graphic presentation as a function of atomic numbers. Rather than measuring all the L transitions of every element, the decision was made to measure and compare relatively strong transitions over a long range of atomic numbers in order to establish the dependence of these transition ratios on atomic numbers.

Figures 3–7 are plots of the indicated measured transition probabilities as a function of the atomic numbers. Also plotted are the experimental values obtained by Victor and by Goldberg, and the theoretical calculation of Scofield. Babushkin's results are also included in all these diagrams except Fig. 5, where the two theories give the same results at low Z and Babushkin's results are only 2% lower than Scofield's at $Z = 92$. Except for $L\gamma_1/L\beta_1$ transition probability ratio where Goldberg's results are extremely large, all experimental values are in some sort of agreement.

In comparing experimental results with theoretical calculations, three main points should be emphasized.

(i) Calculations based on RHFS potenial and screened Coulomb potential are in excellent agreement with experimental results when transitions resulting in a close doublet are compared, i.e, $L\alpha_2/L\alpha_1$ (Fig. 5). Such agreement between theory and experiment has also been observed in the study of the $K\alpha_2/K\alpha_1$ ratios.[30] Good agreement between results based on RHFS potential and experimental values is also observed in the study of the $L\gamma_1/L\beta_1$ transition probability ratio (Fig. 4).

(ii) Discrepancies of about 18% between results based on RHFS potential and experiment are observed in the $Z = 80$ region in the study of $L\beta_3/L\beta_4$ ratio (Fig. 3), and of about 22% in the same region of atomic number in the study of $L\beta_{2,15}/L\alpha_1$ and $L\beta_{2,15}/L\alpha_2$ ratios (Figs. 6 and 7), respectively. Discrepancies of such magnitude were also observed in the K x-ray series,[31] when the energy difference between compared transitions is relatively large. Calculations based on screened Coulomb potential are closer to the experimental results of $L\beta_3/L\beta_4$ ratio throughout the studied spectrum of atomic number and are closer to the experimental results of $L\beta_{2,15}/L\alpha_1$ and $L\beta_{2,15}/L\alpha_2$ ratios for $Z > 75$.

(iii) Figures 4, 6, and 7 show that the experimental values of the indicated transition probability ratios are much larger than the predictions based on the screened Coulomb potential in the region $58 \leq Z \leq 71$. This is conclusive evidence that the change in the slopes of the $L\gamma_1/L\beta_1$, $L\beta_{2,15}/L\alpha_1$, and $L\beta_{2,15}/L\alpha_2$ ratios at about $Z = 70$, predicted

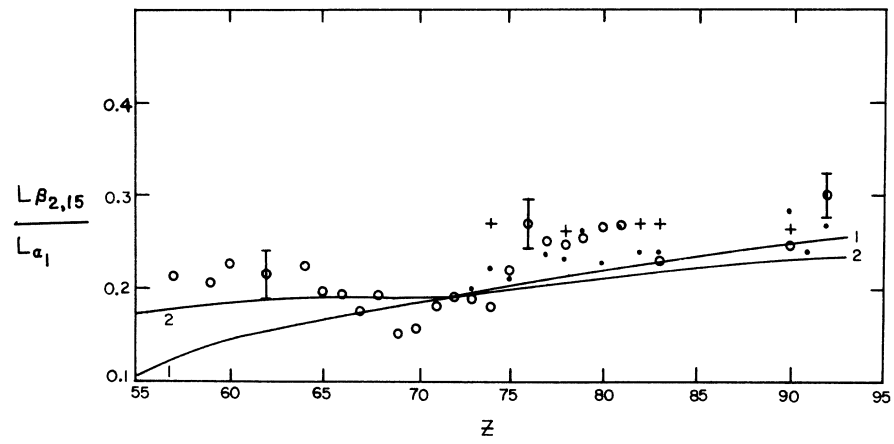

FIG. 6. $L\beta_{2,15}/L\alpha_1$ transition probability ratio as a function of atomic number Z. The curve labels and the symbols have the same designation as in Fig. 3.

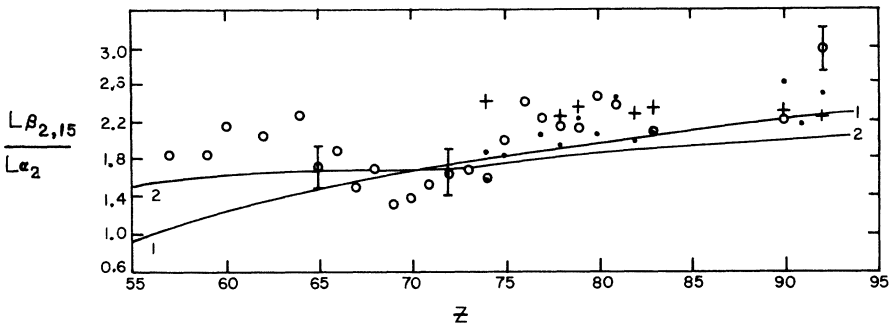

FIG. 7. $L\beta_{2,15}/L\alpha_2$ transition probability ratio as a function of atomic number Z. The curve labels and the symbols have the same designation as in Fig. 3.

on the basis of the RHFS potential, is real, and that the partial filling of the $4f$ electronic level in the region $71 \geq Z \geq 58$ tends to increase the probability of electronic transitions from the $N_{1\nu}$ subshell. Experimental values of the $L\beta_{2,15}/L\alpha_1$ and $L\beta_{2,15}/L\alpha_2$ indicate that the change in the slope of these ratios at about $Z = 70$ is more severe than the predictions of theoretical calculations based on RHFS potential.

CONCLUSION

The present results indicate that the screened Coulomb potential is too coarse to account for the details of the dependence of the transition probability ratios on atomic numbers. Although the agreement between theory and experiment is excellent when doublets of small energy separation are compared, discrepancies of large magnitudes are observed between experimental results and calculations based on RHFS potential, when the energy difference between compared transitions is relatively large.

ACKNOWLEDGMENTS

We wish to thank P. V. Rao, J. M. Palms, and R. E. Wood for supplying their data prior to publication, and F. A. Babushkin for furnishing his numerical results. We acknowledge the helpful assistance of J. V. Hutcherson and R. K. Buchner in the early stages of this project, and thank C. W. Schultz for much of the computer programming. One of the authors, S. I. S., wishes to thank the College administration for the granting of a special leave to conclude this project.

[1]A. Jönsson, Z. Physik 36, 426 (1926).
[2]S. K. Allison, Phys. Rev. 30, 245 (1927); 32, 1 (1928).
[3]V. Hicks, Phys. Rev. 36, 1273 (1930); 38, 572 (1931).
[4]V. J. Andrew, Phys. Rev. 42, 591 (1932).
[5]A. H. Compton and S. K. Allison, *X-Rays in Theory and Experiment* (Van Nostrand, New York, 1935), p. 642.
[6]R. W. G. Wyckoff and F. D. Davidson, Phys. Rev. 36, 1883 (1965).
[7]C. Victor, Ann. Phys. (Paris) 6, 183 (1961).
[8]M. Goldberg, Ann. Phys. (Paris) 7, 329 (1962).
[9]V. Rao, J. M. Palms, and R. E. Wood, Phys. Rev. A 3, 1568 (1971).
[10]H. S. W. Massey and E. H. S. Burhop, Proc. Cambridge Phil. Soc. 32, 461 (1936).
[11]W. Laskar, J. Phys. Radium 16, 644 (1955); Ann. Phys. (Paris) 13, 258 (1958).
[12]W. B. Payne and J. S. Levinger, Phys. Rev. 101, 1020 (1956).
[13]W. N. Asaad, Proc. Roy. Soc. (London) A249, 555 (1959).
[14]G. R. Taylor and W. B. Payne, Phys. Rev. 118, 1549 (1960).
[15]F. A. Babushkin, Acta Phys. Polon. 31, 459 (1967); 25, 749 (1964).
[16]J. H. Scofield, Phys. Rev. 179, 9 (1969).
[17]H. R. Rosner and C. P. Bhalla, Z. Physik 231, 347 (1970).
[18]J. C. Slater, Phys. Rev. 36, 57 (1930).
[19]G. Burns, J. Chem. Phys. 41, 1521 (1964).
[20]S. I. Salem and J. P. Johnson, Phys. Letters 30A, 163 (1969). In this paper, the curves are labeled incorrectly; the one that best fits the experimental points is based on a Coulomb potential screened by Burns's prescription.
[21]S. I. Salem, B. G. Saunders, and G. C. Nelson, Phys. Rev. A 1, 1563 (1970).
[22]D. Liberman, J. T. Waber, and D. T. Cramer, Phys. Rev. 137, A27 (1965).
[23]J. S. Hansen, H. U. Freund, and R. W. Fink, Nucl. Phys. A 142, 604 (1970).
[24]V. D. Mistry and C. A. Quarles, Nucl. Phys. A 164, 219 (1971).
[25]L. G. Parratt, Phys. Rev. 50, 1 (1936).
[25a]S. I. Salem, C. W. Schultz, B. A. Rabbani, and R. T. Tsutsui, Phys. Rev. Letters 27, 477 (1971).
[26]S. I. Salem and D. G. Zarlingo, Phys. Rev. 155, 7 (1967).
[27]S. I. Salem and J. C. Watts, J. Chem. Phys. 39, 2259 (1963).
[28]W. H. McMaster, N. Kerr Del Grande, J. H. Mallett, and J. H. Hubbell, Lawrence Radiation Laboratory Report No. UCRL-50174, Sec. 11, Rev. I, 1969 (unpublished).
[29]R. W. Fink, R. C. Jopson, Hans Mark, and C. D. Swift, Rev. Mod. Phys. 38, 513 (1966).
[30]S. I. Salem and R. J. Wimmer, Phys. Rev. A 2, 1121 (1970).
[31]P. J. Ebert and V. W. Slivinsky, Phys. Rev. 188, 1 (1969); G. C. Nelson, B. G. Saunders, and S. I. Salem, At. Data 1, 377 (1970).